

# Chapter 22

## Wireless Power Delivery Resilient Against Loading Variations



Hiroki Ishikuro

**Abstract** This chapter introduces wireless power delivery systems for battery-less small-size applications. Various kind of new applications such as large volume contactless memory cards or wearable devices will be realized by using wireless power delivery. However, dependability issues should be considered in the wireless power delivery systems for battery-less systems. Small-size low-cost implementation, fast load tracking ability, and reduction of electromagnetic interference (EMI) are typical dependability issues which should be solved. Wireless power delivery technique by inductive coupling is explained at first and several techniques to solve the issues are introduced. For the efficiency improvement, simultaneous power transfer and voltage boosting are tried to eliminate a DC-to-DC converter or charge-pump circuit for data write operation into the flash memory chip. For the fast power control, vector summing of magnetic field and  $\Delta\Sigma$  modulated sub-harmonic switching techniques are explained. For the application of large volume SD card size wireless solid-state drive (SSD), these techniques were implemented into the wireless power delivery system using 0.18  $\mu\text{m}$ -CMOS technology and inductor printed on the PCB board. Experiments with vector summing technique demonstrated a voltage boosting up to 16.3 V at 1 W power transfer with 50% power efficiency. The response time against the load change is 35  $\mu\text{s}$ , which is faster than the conventional system by two orders of magnitude. In the experiments with  $\Delta\Sigma$  modulated sub-harmonic switching technique, power efficiency was improved at low power transmission and spurious emission was suppressed by 8 dB.

**Keywords** Wireless power delivery • Inductive coupling • SSD  
Fast-tracking • EMI

---

H. Ishikuro (✉)  
Keio University, Yokohama, Japan  
e-mail: ishikuro@elec.keio.ac.jp

© Springer Japan KK, part of Springer Nature 2019  
S. Asai (ed.), *VLSI Design and Test for Systems Dependability*,  
[https://doi.org/10.1007/978-4-431-56594-9\\_22](https://doi.org/10.1007/978-4-431-56594-9_22)

## 22.1 Applications and Issues of Wireless Power Delivery Systems

Wireless power transfer technology has long history and is put into practical use from 1990s. Battery charging for cordless phone or electrical toothbrush is one of such application and RF-ID tag is another successful application of wireless power delivery. These applications use inductive coupling. In the case of battery charging, strongly coupled inductors are used for watt-class power transfer. For the RF-ID tag, loosely coupled inductors are used and power efficiency is very low. However, the required power is very small and the low efficiency does not become problem. To improve the power efficiency in the weakly coupled system, wireless power transfer which uses magnetic resonance has been proposed [1, 2] and attract much attention for the application of battery charging for electric car. Wireless power transfer using microwave and directional antenna [3] is the other technique, which makes it possible to deliver electric power over a long distance.

Recently large volume nonvolatile memory devices such as solid-state drive (SSD) play more and more important roles in computer system or information appliance. Such devices are connected with the host by wire to transfer the data and power. If the power and data can be transferred by wireless, the connector and cable can be eliminated (Fig. 22.1a). This brings dependability to the system because it can become waterproof and free from contact failure. It also brings flexibility to the system design.

According to the roadmap of SD Association [4], 2T byte volume with bus speed of 312 Mbps is standardized for the specification of future SD card. As described previously, many researches on the wireless power transfer which used inductive coupling [5] or magnetic resonance [1, 2] have been reported. Wireless power transfer standard such as “Qi” [6] has been established and several products have already been in commercial use. In such application, secondary side (receiver side) contains battery and it acts as a buffer which hides rapid secondary side load variation from primary side, hence, fast power control is not required.

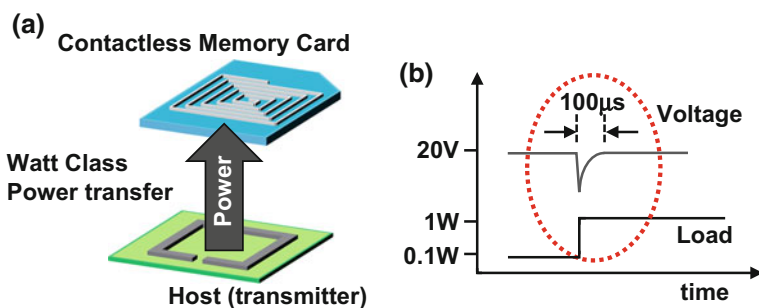


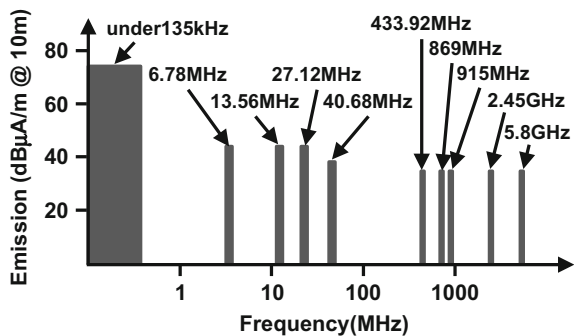
Fig. 22.1 Wireless power delivery for large volume memory card

However, for the application of the wireless memory card, it is not practical to contain a battery in the card. Therefore, the rapid load change in the card may disturb the voltage (Fig. 22.1b) and degrade the circuit operation or device reliability. As used in the RF-ID cards [7], shunt regulator (voltage limiter) can suppress the voltage variation in the card by consuming overloaded power. In the case of RF-ID, because circuits consume only milli-watt order power, the power efficiency is not important. Thus, it is enough to use shunt regulator at secondary side. However, the peak power of the future terra-byte class memory devices becomes watt class and the heat generated in the regulator degrades system reliability. To avoid such problem, high-speed power control is inevitable. Commonly used watt-class wireless power delivery systems, for example, Qi standard contains the battery at secondary side, and rapid load change does not occur. Therefore, these systems usually chose several hundred kHz for switching frequency, which is not sufficient for quick response to load variation. To achieve high-speed power control, MHz band frequency is suited. However, if the wireless power transfer uses MHz band frequency, the allowed frequency band (ISM band Industrial, Scientific and Medical (ISM) band) is narrow (Fig. 22.2) [7], and frequency modulation cannot be used for power control. For example, the available frequency range for the 6.78 MHz band is  $\pm 15$  kHz and for the 13.56 MHz band is  $\pm 7$  kHz.

Another requirement in the contactless memory card is a voltage boosting for data write operation. In the flash memory chip, charge-pump circuit is embedded to generate a high voltage. However, charge pump consumes about 60% of power during write operation in NAND flash memory chip [8]. To improve the efficiency, DC-to-DC converter can be used. However, the additional components are required which increases the size and cost of the card.

From the next section, wireless power transfer techniques with voltage boosting which is developed [9, 10] for compact size battery-less applications are introduced. Although the motive application is SD card size wireless memory card, these techniques can be utilized for wide variety of applications such as wearable devices or medical implantable devices.

Fig. 22.2 Frequency chart of ISM band



## 22.2 Wireless Power Delivery by Inductive Coupling

In general, wireless power delivery system by inductive coupling consists of a transmitter, strongly coupled inductors, and a rectifier (Fig. 22.3). The transmitter converts input DC voltage to AC signal by switching transistors. The AC signal drives the transmitting inductor and magnetic field is induced by the AC current in the inductor. In the receiver side, AC voltage is induced in the receiving inductor and the AC voltage is rectified to generate DC output voltage. Since the coupling coefficient between the transmitting and receiving inductor is lower than one (typically 0.5 at most), leakage inductances impede the AC current flow through the inductors. To cancel these leakage inductances, capacitors are usually placed in parallel or in series with the inductors and the resonant frequency is tuned at switching frequency.

For battery charging applications, such as electric toothbrush or recent Qi standard, the switching frequency of several hundred kHz is usually used. Since there is a battery in the receiver side, the load variation is gradual and fast power control is not required for these applications. The transmitting power is controlled by frequency modulation. Since the LC tuned inductors are used, the transmitting power becomes maximum when the switching frequency is set at resonant frequency. If the switching frequency is de-tuned from resonant frequency, the transmitting power is reduced.

As mentioned in the previous section, fast power control is required for watt-class battery-less application. If the MHz band is used for switching frequency, allowed frequency band is very narrow and usual frequency modulation cannot be used for power control. Furthermore, EMI should be suppressed even when the transmitting power is rapidly controlled.

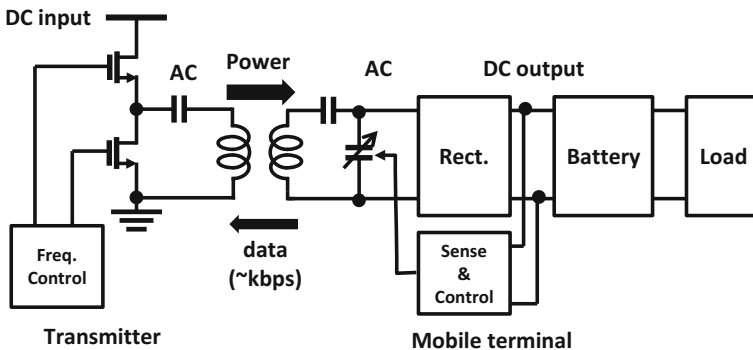


Fig. 22.3 Wireless power delivery system by inductive coupling

### 22.3 Approach for Power Efficiency Improvement and Size Reduction

In the application of large volume memory card, NAND flash memory requires high voltage during data write operation. Figure 22.4a shows one example to boost the secondary side voltage for this kind of application. As described previously, frequency modulation cannot be used for transmitting power control in the wireless power delivery system which uses MHz band. Therefore, in the primary side, DC-to-DC converter which adjusts input DC voltage should be placed to control the transmitting power. The driver circuit (TX) converts the DC to AC current. At secondary side, rectifier converts AC to DC voltage again, and DC-to-DC converter or charge-pump circuit boosts the voltage to required level for data write operation. Total efficiency can be written as,

$$\eta_{Total} = \eta_{DC-DC Converter} \times \eta_{TX} \times \eta_{Coil} \times \eta_{Rectifier} \times \eta_{Boost Circuit} \tag{22.1}$$

Since every component has a power loss, the total efficiency becomes low. For example, it has been reported that the power efficiency of DC-to-DC converter for controlling input-voltage is about 93% [11]. And, power efficiency of the charge pump for nonvolatile memory decreases with increased ratio of voltage boosting. If voltage boosting ratio is larger than 5, the reported power efficiency of the charge-pump circuit is 53% [12]. Furthermore, if the rectification in the receiver is carried out before voltage boosting, the power loss in the rectifier becomes large because the voltage drop by the diode is relatively large. The rectifier loss can become approximately 25% if the rectifier output voltage is 3.3 V. As a result, Eq. (22.1) becomes

$$\eta_{Total} = 0.93 \times \eta_{TX} \times \eta_{Coil} \times 0.75 \times 0.53 = 0.37 \times \eta_{TX} \times \eta_{Coil}.$$

Furthermore, the DC-to-DC converter or charge pump increases the number of discrete components, cost, and module size.

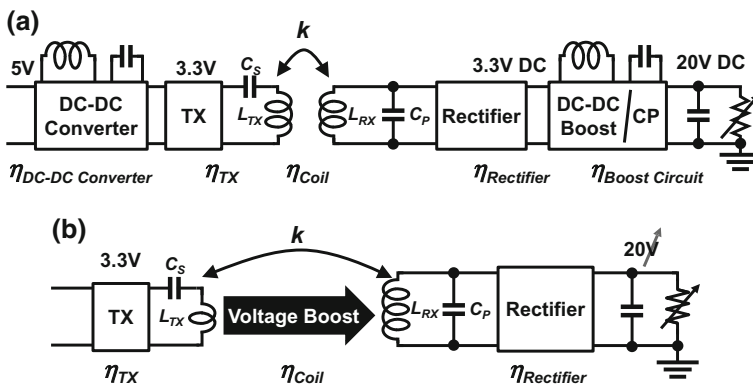


Fig. 22.4 Wireless power delivery system for improved power efficiency and reduced module size

Figure 22.4b shows an architecture to improve the power efficiency and reduce the module size. Instead of voltage boosting by DC-to-DC converter or charge-pump circuit, the secondary side voltage is boosted by using inductors with large winding number ratio between the primary and secondary inductors. The advantage of this approach is the reduced number of components which brings an improved efficiency and therefore, reduced size and cost. The total power efficiency can be given as,

$$\eta_{Total} = \eta_{TX} \times \eta_{Coil} \times \eta_{Rectifier}. \quad (22.2)$$

In this approach, the winding number ratio between the transmitter and receiver inductors becomes large for voltage boosting. Thus, it is thought that transmission efficiency falls about several percent. However, since the DC-to-DC converter and charge pump can be removed, overall efficiency improves. Moreover, in rectifier circuit, the relative voltage drop by the diode is small because the voltage is boosted prior to the rectification. The loss by the rectifier can be reduced to 7.3%. Therefore, the Eq. (22.2) can be rewritten as

$$\eta_{Total} = \eta_{TX} \times \eta_{Coil} \times \eta_{Rectifier} = \eta_{TX} \times \eta_{Coil} \times 0.93.$$

The issue of this approach is that some techniques to rapidly control the transmitting power is required without using DC-to-DC converter or frequency modulation. Several kinds of techniques can be used to solve this issue and two techniques are introduced in the next section.

## 22.4 Fast Load Tracking and EMI Reduction Technique

### 22.4.1 Vector Summation of Magnetic Fields

Figure 22.5 shows a transmitting power control by vector summing of magnetic fields [9]. The transmitter consists of two drivers and coils which forms two half-bridge configurations in this figure. The phase difference between the switching clocks in each driver introduces the phase difference between the current in each inductor. The induced magnetic fields are summed in the secondary inductor. The power contribution from each primary coils ( $L_{TX1}$  and  $L_{TX2}$ ) is  $P_O$  and  $P_O e^{j\theta}$ , respectively and secondary power can be expressed as,

$$Power = P_O \times (1 + \cos \theta). \quad (22.3)$$

Same kind of power control technique which uses a full-bridge structure with phase shift PWM has been proposed [13]. By shifting the phase of the switching clocks, the duty ratio when the current flow through the transmitting inductor can be changed and the transmitting power can be controlled. However, the current flows

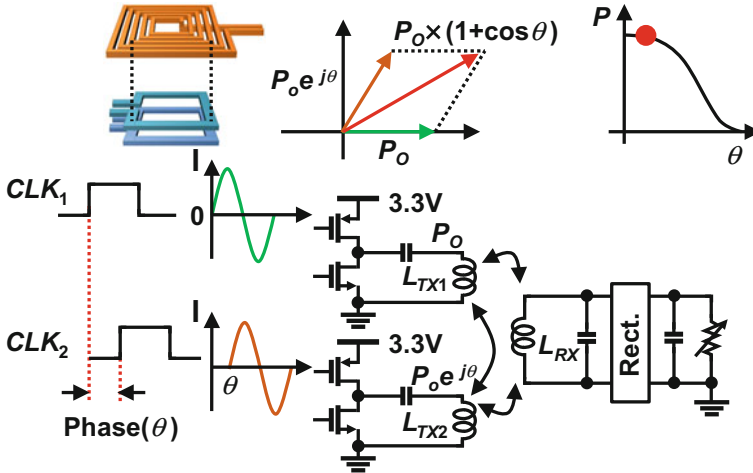


Fig. 22.5 Power control by vector summing of magnetic fields

through both PMOS and NMOS at the same time. Since the voltage is boosted by using large winding number ratio, the primary inductor for the application of wireless memory card has only one turn. Therefore, parasitic resistances of MOSFETs bring severe power loss. In the half-bridge configuration, current flows through only PMOS or NMOS at the same time, thus, reduces power loss. Furthermore, using two half-bridge configurations reduces the required current in one transistor to half. In standard CMOS technology, it is difficult to transfer high power because large current becomes stress for MOSFET and degrades its characteristics. Therefore current reduction in one transistor becomes advantage.

### 22.4.2 Sub-harmonic Switching Technique

The other technique for the fast transmitting power control is switching frequency control between fundamental and sub-harmonic of resonant frequency [10].

Figure 22.6 shows the operation principle of the power control by sub-harmonic switching. Both the transmitter and receiver use LC resonant circuits to improve the power efficiency. To transmit maximum power, the output driver is driven by a clock signal at  $f_{res}$  (resonant switching mode) (Fig. 22.6a). When the high-side switch is on ( $\phi_1$ ), the current begins to flow into the inductor and converted to the magnetic field energy. Since the LC resonance is used, the inductor current begins to decrease at quarter cycle and becomes zero at half cycle of  $f_{res}$ . At this moment ( $\phi_2$ ), the high-side switch is off and low-side switch is on. The current flows through the loop formed by an inductor, capacitor, and low-side switch. In this sequence, rectangular voltage waveform whose fundamental frequency is same as

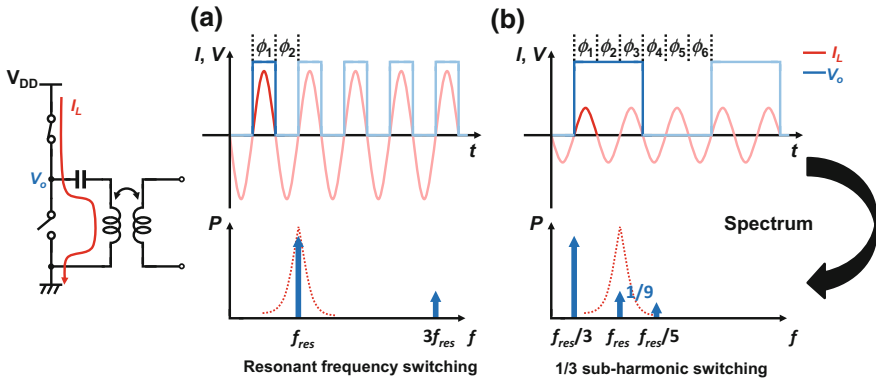


**Fig. 22.6** Transmitting power control by resonant/sub-harmonic switching

$f_{res}$  is applied to LC resonant circuit. Since the conductance of the LC circuit is maximum at resonant frequency and becomes small at the other frequency, the current flow through the LC circuit is in proportion to the fundamental component of the rectangular voltage form. The harmonic components of the rectangular waveform are suppressed.

If the switching frequency is set at  $f_{res}/3$  (sub-harmonic switching mode) (Fig. 22.6b), the power is transferred in the following way. From phase  $\phi_1$  to  $\phi_3$ , the high-side switch is on and low-side switch is off. During the phase  $\phi_1$ , the current flows from power supply to the inductor. Then, at phase  $\phi_2$ , the current flows back to the power supply, and at  $\phi_3$ , the current flows again from the power supply. From phase  $\phi_4$  to  $\phi_6$ , the high-side switch is off and low-side switch is on. The current flows back and forth in the loop formed by the inductor, capacitor, and low-side switch. The energy dissipated by the receiver is refilled at every three cycles of  $f_{res}$  and transmitting power can be reduced. This can be explained in the frequency domain in the following way. The fundamental component of the rectangular voltage waveform cannot excite the current in the LC circuit because the conductance of the LC circuit at this frequency is small. On the other hand, the third harmonics of the rectangular waveform coincides with the resonant frequency of the LC circuit and excite the current in the LC circuit. Since the voltage amplitude of the third harmonics is one-third of the fundamental components, the transmitted power is one-ninth of that of the resonant switching.

By changing the ratio between the switching by  $f_{res}$  and  $f_{res}/3$ , the transmitted power can be continuously controlled. Different from FM or PWM, the frequency of the current flowing through the inductor is close to  $f_{res}$  and zero current switching is achieved in both the switching mode. This dramatically reduces the unwanted spurious emission.

To further reduce the spurious emission, a  $\Delta\Sigma$  modulator is adopted to generate the control signal to change between the resonant switching and sub-harmonic switching mode as shown in Figs. 22.7 and 22.8.



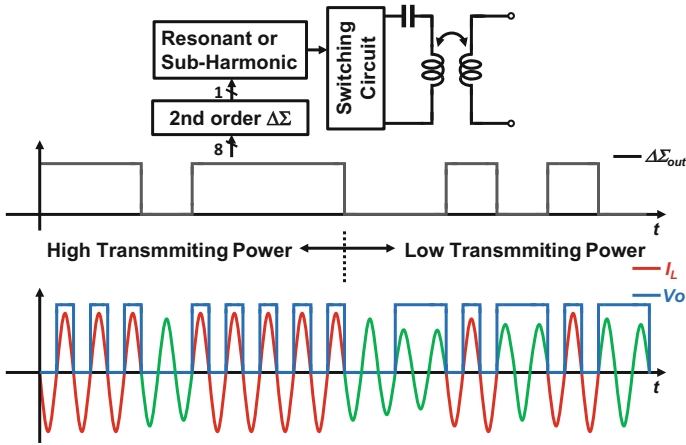


Fig. 22.7 EMI reduction by ΔΣ modulation of resonant and sub-harmonic switching

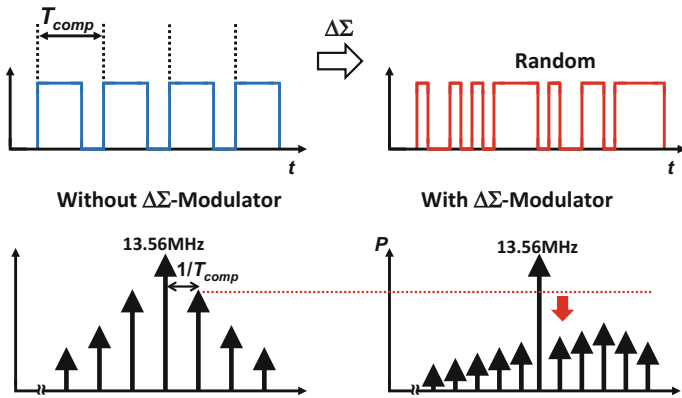


Fig. 22.8 Spur spreading by ΔΣ modulation of resonant and sub-harmonic switching

## 22.5 Wireless Power Delivery System Implementation

### A. System Overview

Figure 22.9 shows block diagram of the developed power transfer system for large volume memory card. The metal layers in the PCB are used for transmitting and receiving inductor. Phase difference between the switching clocks for primary coils  $L_{TX1}$  and  $L_{TX2}$  is controlled by Delay Locked Loop (DLL). Then, dead time generator inserts the non-overlap phase between the switching clocks for PMOS and NMOS to prevent  $V_{DD}$  and  $GND$  from being shorted. The resonant frequency of the primary inductors is tuned by series LC connection.

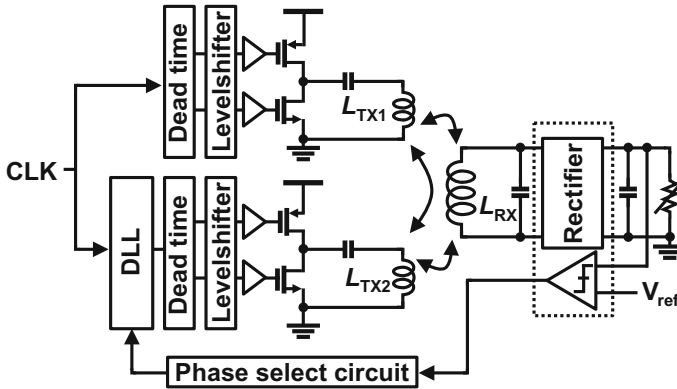


Fig. 22.9 System block diagram of the wireless power delivery for large volume memory card

Considering the SD card size, diameters of the transmitting and receiving inductors are about 20 mm. The turn number of primary and secondary inductors are one and eight, respectively. The self-inductance of primary ( $L_{TX}$ ) and secondary inductor ( $L_{RX}$ ) are 41 nH and 2.58  $\mu$ H, respectively. The distance between the primary and secondary inductors are several millimeter.

In the secondary side, parallel LC connection is adopted to tune the resonant frequency. Since the parallel connected LC circuit acts as current source at resonant frequency, high voltage can be obtained, making it suitable for voltage boosting. The gate cross-coupled rectifier is used to convert from AC to DC voltage. The generated DC voltage is compared with the reference voltage and fed back to the DLL for power control.

### B. Series-Parallel Resonance Link Design

At primary side, transmitting inductors  $L_{TX1}$  and  $L_{TX2}$  are the same size. On the other hand, the distances between the primary and secondary inductors are much longer than the distance between each primary inductors. To improve the power transfer efficiency, reactance component of each leakage inductance should be canceled by capacitors at switching frequency.

As explained in Fig. 22.2, several frequencies can be used for wireless power delivery as ISM band. Considering that the tradeoff between the response speed, components size, and power transfer efficiency, the switching frequency of 6.78 MHz or 13.56 MHz becomes a candidate for this application. If the higher switching frequency is chosen, the response speed for power control can be improved and component size can be decreased. However, the power transfer efficiency degrades by the charge and discharge through parasitic capacitance and resistance of MOSFETs. If lower frequency is chosen, the power efficiency can be increased. In this work, placing the emphasis on the efficiency, the resonant frequency of primary and secondary inductors are tuned at 6.78 MHz. The capacitances

for resonance in the primary side are determined as 14 and 13 nF, and secondary side is determined as 220 pF.

Using Electromagnetic field solver simulator, each parasitic resistor is obtained. The primary side’s parasitic resistance ( $R_{main1}$ ,  $R_{main2}$ ) is 70 mΩ, while the secondary side ( $R_{main3}$ ) is 3 Ω.

C. Rectifier

Gate cross-coupled rectifier [14] is adopted. Figure 22.10 shows rectifier circuit. Thick oxide lateral-diffused MOS (LDMOS) with maximum rated voltage of 32 V are used. At secondary side, induced voltage between the coil terminals is high because of voltage boosting,  $V_{GS}$  of gate cross-coupled NMOS becomes large and on-resistance of NMOS is low. As a result,  $V_{DS}$  of NMOS is also low and parasitic diode in NMOS does not turn on. Therefore, no additional dynamic bulk regulation transistors are necessary for switch NMOS, which improves rectifier efficiency. Reducing the dropout voltage by PMOS of the rectifier improves power efficiency in the rectifier circuit and increases the rectified dc voltage  $V_{rect\_out}$ .

To minimize the dropout voltage and improve power efficiency, the W/L ratio is increased as large as the chip area permitted.

E. Feedback Control

In this system, bang-bang control is adopted. At initial state, to prevent break down of the MOSFETs and device connected to this wireless power delivery system, phase difference between the switching clocks for primary coils is start from 180° (minimum transmitting power). Then, the rectified output voltage is compared with the reference voltage and fed back to the phase select circuit of the DLL.

During the system start-up, the output voltage of the rectifier is lower than the target voltage. At first, the counter is set at its maximum count level. To increase the transmitting power, the phase select circuit decrements the counter and reduce the phase difference. The counter and phase difference is reduced every cycle until

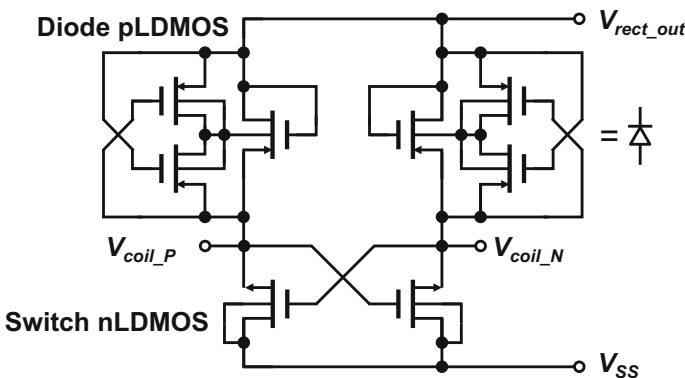


Fig. 22.10 Rectifier circuit in the secondary side

the output voltage reaches the target voltage. Once the output voltage exceeds the target voltage, the phase select circuit increments the counter and increase the phase difference. As a result, the transmitted power and output voltage of the rectifier is decreased. Since the phase control signal is updated at every cycle of clock, the transmitter can reach its maximum power setting within 32 clock cycles from start-up.

When load variation occurs, the output voltage of the rectified changes. When the power consumption of the load decreases, the required power reduces. The phase control circuit increases the phase difference to reduce the transmitting power. On the other hand, if the power consumption of the load increases, the phase control circuit reduces the phase difference to increase the transmitting power. As a result, the output voltage becomes constant value against the load variation.

## 22.6 Experimental Results

Figure 22.11a, b are power transceiver modules and Fig. 22.12a, b are test chip microphotographs. An 0.18  $\mu\text{m}$ -CMOS process with high-voltage LDMOS option was used. Low voltage (1.8 V) MOSFETs are used for DLL and other control circuit. Medium voltage (5 V) MOSFETs are used as switching driver circuit and high-voltage (32 V) LDMOSFETs are used in secondary circuit. The inductor size in the PCB board is 20 mm  $\times$  20 mm. The chip size of both the transmitter and rectifier are 2.5 mm  $\times$  2.5 mm.

In the experiment, distance between the primary and secondary inductors is set at 1 mm. Switching frequency is 6.78 MHz.

Figure 22.13 shows the relation between the receiver power and clock phase of the DLL. 50% efficiency and 1 W power delivery at 266  $\Omega$  load is achieved. Power can be controlled while keeping the efficiency about 40% across the range of max-to-half power. Figure 22.14 shows the output voltage with and without power

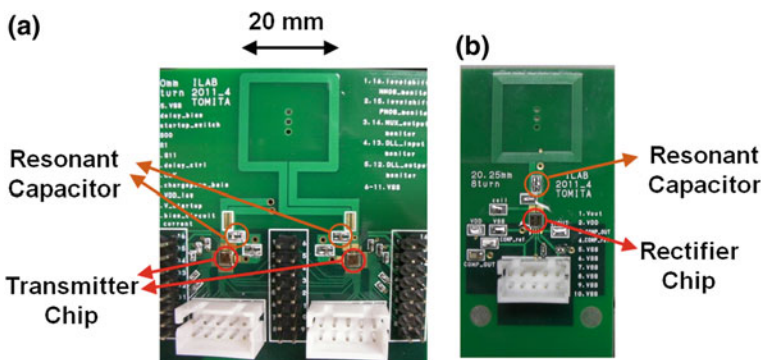


Fig. 22.11 Power transmitter and receiver module

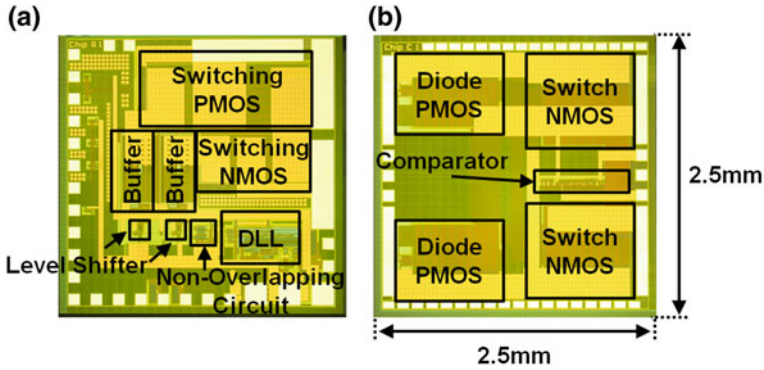


Fig. 22.12 Fabricated test chip in 0.18  $\mu\text{m}$ -CMOS with high-voltage LDMOS option, **a** transmitter chip, **b** rectifier chip

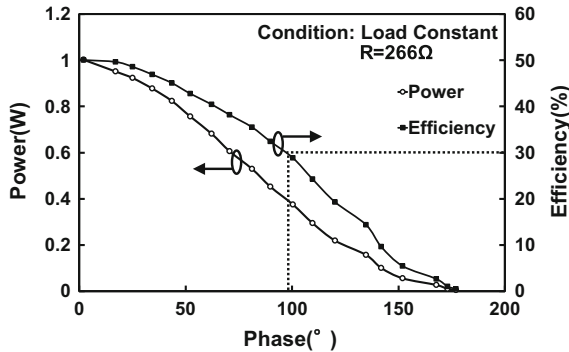


Fig. 22.13 Relation between receiver power and phase difference of switching clocks of two transmitters

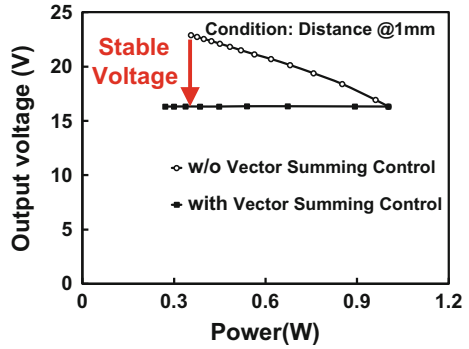
control when the secondary side load is changed. By controlling the transmitting power, the secondary side voltage can be stabilized.

Figure 22.15 shows the measured transient response of the power control loop. Even when the secondary side load is changed from 71 mW to 1 W, the voltage drop is only 2.7% and it takes only 35  $\mu\text{s}$  to recover the output voltage. This response time about 100 times faster than that in the wireless power transceiver for “Qi” standard.

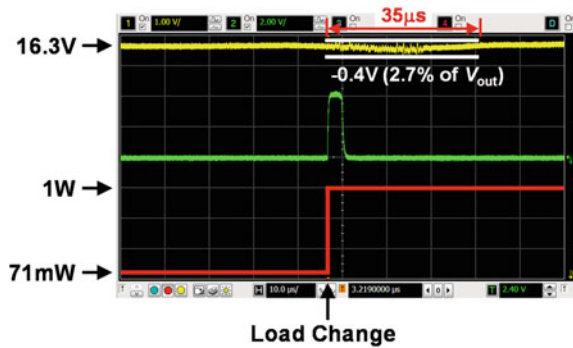
In the previous experiments which used vector summing of two transmitters, the power efficiency becomes low when the transmitted power is small. Most of the time in the operation, memory card consumes power much lower than the peak power. Therefore, power efficiency at lower transmitting power is also important.

The other experiments which used power control by  $\Delta\Sigma$  modulated switching between fundamental and sub-harmonic resonant frequency was carried out. In this

**Fig. 22.14** Voltage regulation by vector summing of two transmitters



**Fig. 22.15** Transient response when the load is changed from 71 mW to 1 W



experiment, only one transmitter was used. The power supply voltage is 1.8 V for controller and 3.3 V for class-D amplifier. The middle voltage (5 V) MOSFETs are used for level shifter and class-D amplifier. LC resonant circuit was tuned at 13.56 MHz. The clock frequency is switched between 13.56 MHz (fundamental) and 4.52 MHz (sub-harmonic) for resonant switching and sub-harmonic switching, respectively. At the output of the rectifier, a comparator is placed to detect the rectified voltage. All the circuits in receiver side are designed using high-voltage LDMOS with rated voltage of 32 V. The off-chip capacitor to remove the ripple has capacitance of 33 nF. The comparator output signal is fed back to the loop filter and  $\Delta\Sigma$  modulator in the transmitter side.

Figure 22.16 shows the measured relation between the transmitted power and total power transmission efficiency as a function of power setting code. In this experiment, the distance between the transmitter coil and receiver coil is set at 5 mm. Maximum power of 0.52 W can be delivered with an efficiency of 50%. The transmitted power range is wider than one order of magnitude. Compared with the previously mentioned experimental results (Fig. 22.13) the relation between the transmitted power and setting code has good linearity which enables the simple design of feedback loop. Furthermore, reasonable efficiencies are maintained over the power setting.

**Fig. 22.16** Power setting code versus transferred power and total power efficiency

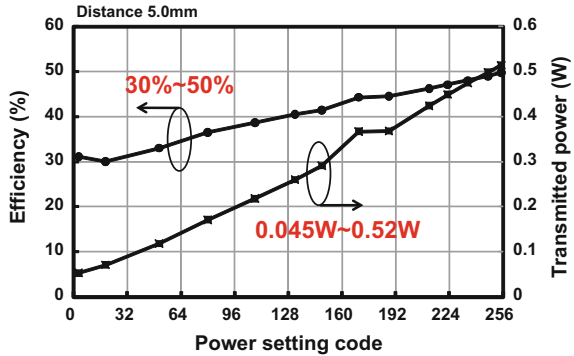


**Fig. 22.17** Spurious emission level as a function of power setting code

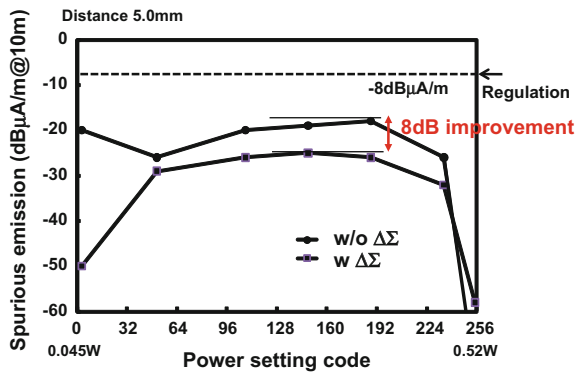


Figure 22.17 shows the spurious emission level from the developed wireless power delivery system. For the comparison, the spurious emission levels with and without  $\Delta\Sigma$  modulator are plotted. In each case, the worst level spurious tone is chosen. The  $\Delta\Sigma$  modulator suppresses the spurious tone by 8 dB and spurious tone meets the regulation with enough margin.

## 22.7 Summary

Wireless power delivery system for battery-less application was introduced. As dependability issues for this kind of power delivery system, the requirement of fast load tracking ability and EMI suppression were discussed. To realize the fast load tracking and EMI suppression, rapid power control techniques with vector summing of magnetic field and  $\Delta\Sigma$  modulated sub-harmonic resonant frequency switching were introduced.

Aiming the application of large volume SD card size wireless memory card (SSD), voltage boosting wireless power transfer system with the above-mentioned

techniques were developed using 0.18  $\mu\text{m}$ -CMOS and printed inductors in PCB board. The size of the inductors are 20 mm  $\times$  20 mm and test transceiver chip is 2.5 mm  $\times$  2.5 mm. Experiments with vector summing technique demonstrated a voltage boosting up to 16.3 V at 1 W power transfer with 50% power efficiency. The response time against the load change is 35  $\mu\text{s}$  which is faster than the conventional system by two orders of magnitude. In the experiments with  $\Delta\Sigma$  modulated sub-harmonic switching technique, power efficiency was improved at low power transmission and spurious emission was suppressed by 8 dB.

## References

1. A. Kurs, A. Karalis, R. Moffatt, J.D. Joannopoulos, P. Fisher, M. Soljačić, Wireless power transfer via strongly coupled magnetic resonances. *Science* **317**, 83 (2007)
2. T.C. Beh, T. Imura, M. Kato, Y. Hori, Basic study of improving efficiency of wireless power transfer via magnetic resonance coupling based on impedance matching, in *IEEE International Symposium on Industrial Electronics Dig* July, 2010, pp. 2011–2016
3. R.M. Dickinson, Power in the sky: requirements for microwave wireless power beamers for powering high-altitude platforms. *IEEE Microwave Mag.* **14**(2), 36–47 (2013)
4. SD Association, <https://www.sdcard.org/home/>
5. A. Radecki, H. Chung, Y. Yoshida, N. Miura, T. Shidei, H. Ishikuro, T. Kuroda, 6W/25mm<sup>2</sup> inductive power transfer for non-contact wafer-level testing, in *IEEE ISSCC Dig*, Feb, 2011, pp. 230–232
6. Wireless Power Consortium, *Qi System Description Wireless Power Transfer Volume I: Low Power Part 1: Interface Definition Version 1.0.2*, April, 2011, pp. 1–50
7. K. Finkenzerler, *RFID HANDBOOK*, 2nd edn. (Translated by R. Waddington), Munich/FRG, original German language published by Carl Hanser Verlag, The Atrium/Southern Gate/Chichester/West Sussex PO19 8SQ/England (Wiley, 2003), pp. 161–181
8. K. Ishida, T. Yasufuku, S. Miyamoto, H. Nakai, M. Takamiya, T. Sakurai, K. Takeuchi, 1.8V Low-transient-energy adaptive program-voltage generator based on boost converter for 3D-integrated NAND flash SSD. *IEEE J. Solid-State Circuits* **46**(6), 1478–1487 (2011)
9. K. Tomita, R. Shinoda, T. Kuroda, H. Ishikuro, 1W 3.3V-to-16.3V Boosting wireless power transfer circuits with vector summing power controller. *IEEE J. Solid-State Circuits* **47**(11), 2576–2585 (2012)
10. R. Shinoda, K. Tomita, Y. Hasegawa, H. Ishikuro, Voltage-boosting wireless power delivery system with fast load tracker by  $\Delta\Sigma$ -modulated sub-harmonic resonant switching, in *IEEE International Solid-State Circuits Conference (ISSCC)* Feb, 2012, pp. 288–290
11. C. Zheng, D. Ma, A 10-MHz green-mode automatic reconfigurable switching converter for DVS-enabled VLSI systems. *IEEE J. Solid-State Circuits* **46**(6), 1464–1477 (2011)
12. A. Richelli, L. Mensi, L. Colalongo, P.L. Rolandi, Z.M. Kovacs-Vajna, A 1.2-to-8V Charge-pump with improved power efficiency for non-volatile memories, in *IEEE ISSCC Dig*, Feb, 2007, pp. 522–619
13. T. Ishii, H. Kakehashi, H. Ogasawara, T. Ninomiya, Piezoelectric-transformer inverter with full-bridge phase-shift control scheme, in *Institute of Electronics Information and Communication Engineers Dig*, Nov, 1999, pp. 45–51
14. M. Ghovanloo, K. Najafi, Fully integrated wideband high-current rectifiers for inductively powered devices. *IEEE J. Solid-State Circuits* **39**(11), 1976–1984 (2004)